Excitation-autoionization in highly charged sodiumlike ions

K. J. Reed and M. H. Chen
High Temperature Physics Division, Lawrence Livermore National Laboratory, Livermore, California 94550

D. L. Moores
Department of Physics and Astronomy, University College London, Gower Street, London, WCIE 6BT, England
(Received 24 May 1991)

The effects of excitation-autoionization have been studied for nine sodiumlike ions with $26 \leq Z \leq 92$. Relativistic-distorted-wave methods were used to calculate cross sections for direct electron-impact ionization of these ions. Relativistic-distorted-wave cross sections were computed for electron-impact excitation of $n=2$ electrons to $n=3$ levels of the ions, and detailed relativistic Auger rates and radiative rates were calculated in order to obtain the excitation-autoionization cross sections. We investigated the variation of these cross sections along the Na-like isoelectronic sequence. We found that configuration interaction significantly affects some cross sections in ions where level crossings occur for some of the doubly excited intermediate states.

PACS number(s): 34.80.Kw

INTRODUCTION

In recent papers we have discussed the effects of indirect processes on electron-impact ionization of several highly charged sodiumlike ions [1–3]. Earlier theoretical and experimental studies of electron-impact ionization of lighter sodiumlike ions demonstrated that excitation-autoionization significantly enhances the direct ionization cross sections for ions with $Z \leq 28$ [4–9]. More recent studies of Au^{68+} indicated that substantial excitation-autoionization effects persist for heavier Na-like ions, contrary to an earlier expectation that radiative decay would render these effects negligible in high-Z ions [1]. Subsequent calculations indicated similar excitation-autoionization enhancement of electron-impact ionization of Na-like Xe [3]. These theoretical results for Xe^{43+} were in good agreement with reported measurements of electron-impact ionization cross sections for incident electron energies between 8 and 15 keV [10,11], and were further substantiated by recent measurements using an electron beam ion trap, for incident electron energies between 4 and 8 keV [12]. In these heavy Na-like ions the enhancement results largely from excitation to a few intermediate states which have large excitation cross sections and also large probabilities for Auger decay. It was also shown (in Refs. [1,2]) that it is necessary to carry out detailed calculations of excitation cross sections and branching ratios for each intermediate state since the contributions of these few levels could be missed if averaging techniques are used in place of detailed calculations. Detailed calculations of excitation-autoionization and resonant-excitation double autoionization in Fe^{15+} shed light on a long-standing discrepancy between earlier theoretical and experimental results [2].

In this paper we discuss excitation autoionization for nine sodiumlike ions with $26 \leq Z \leq 92$. In addition to our earlier calculations for Au^{68+}, Xe^{43+}, and Fe^{15+}, we have calculated direct ionization cross sections, excitation cross sections, and branching ratios for Se^{23+}, Mo^{31+}, Ag^{36+}, Ba^{45+}, Eu^{52+}, and U^{81+}. These particular elements were chosen because of their possible use in future experiments on the electron beam ion trap at Lawrence Livermore National Laboratory. In addition, highly charged ions of selenium play an important role in soft-x-ray laser experiments [13]. We investigate the variation of excitation-autoionization effects along the Na-like isoelectronic sequence, and, in particular, we examine how the contributions of certain intermediate states vary with atomic number. We restrict our investigation to energy regimes where the effects of direct ionization of the $2p$ and $2s$ electrons are not significant. Contributions from excitation of inner-shell electrons to $n=4$ states of the ions are also unimportant.

THEORETICAL METHOD

Our calculational procedure has been described in detail in Refs. [1–3]. Briefly we carried out separate fully relativistic calculations of the direct ionization cross sections (Q_d), the cross sections for excitation to the intermediate autoionizing states (Q_i), and the radiative and Auger rates for decay of the intermediate states. The following processes were considered for each ion:

$$2s^2 2p^6 3s + e \rightarrow 2s^2 2p^6 + e + e \ , \quad (1)$$

$$2s^2 2p^6 3s + e \rightarrow 2s^2 2p^5 3s 3l + e \rightarrow 2s^2 2p^6 + e + e \ , \quad (2)$$

$$2s^2 2p^6 3s + e \rightarrow 2s^1 2p^6 3s 3l + e \rightarrow 2s^2 2p^6 + e + e \ , \quad (3)$$

$$2s^2 2p^6 3s + e \rightarrow 2s^2 2p^5 3p^2 + e \rightarrow 2s^2 2p^6 + e + e \ . \quad (4)$$

Most of the direct ionization cross sections were calculated using a full partial wave approximation [14] in which the bound, incident, scattered, and ejected electrons are computed in Dirac-Fock potentials. In some cases direct ionization cross sections were computed using a relativistic-distorted-wave method developed by

Zhang and Sampson [15]. The two methods give essentially identical ionization cross sections for sodiumlike ions.

A relativistic-distorted-wave method was used to compute the cross sections for exciting the $2s$ and $2p$ electrons to the $n=3$ subshells. Relativistic configuration-interaction wave functions for the target ions were generated using a Dirac-Fock atomic structure code developed by Hagelstein and Jung [16]. In the target structure for each ion included all of the $2s^2 2p^6 3l$, $2s^2 2p^5 3l 3l'$, and $2s^1 2p^6 3l 3l'$ $(l,l'=0,1,2)$ configurations. Partial waves up to $l=14$ were sufficient to converge the cross sections for electric-dipole-forbidden transitions. For the dipole-allowed transitions partial waves up to $l=90$ were computed. The Auger branching ratio B_i for intermediate state i is given by

$$B_i=\frac{\sum_j A_{ij}^a}{\sum_j A_{ij}^a+\sum_k A_{ik}^r} . \tag{5}$$

Here A_{ij}^a is the probability for an excited state i to autoionize to state j and A_{ik}^r is the probability for radiative decay of excited state i to state k. In our earlier work [1–3], radiative transitions among autoionizing states were assumed to be small and were neglected. In order to assess the validity of this approximation we included radiative transitions among autoionizing states for some ions studied in this work. The effects of including these radiative transitions are discussed in the next section. The detailed Auger and radiative rates were calculated using the multiconfiguration Dirac-Fock model (MCDF) [17,18]. The energy levels and wave functions for the excited states were calculated explicitly in intermediate coupling, including configuration interaction within the same complex using the MCDF model in the average-level scheme [16]. Assuming that the excitation-autoionization processes and the direct ionization process are independent, the total cross section Q_t is then given by

$$Q_t=Q_d+\sum_i Q_i B_i . \tag{6}$$

RESULTS AND DISCUSSIONS

We computed excitation cross sections and branching ratios for 80 intermediate states for each ion. Most of the intermediate states make very little contribution to the ionization cross sections because either their excitation cross sections or branching ratios are very small. We refer to the product $Q_i B_i$ as the excitation-autoionization cross section for intermediate state i. In Table I we list the intermediate states which have the ten largest excitation-autoionization cross sections for each of the ions. The excitation-autoionization cross sections shown in the tables are computed at an incident electron energy slightly above the excitation threshold for the highest intermediate state so that all of the excitation channels are open. The level indices in each table refer to the ordering of all states in the target structure calculation for the ion in that table. Each state is identified by the dominant component in the j-j basis set. In our configuration notation the first orbital in the configuration is the inner shell having a vacancy. The last two numbers give the outer-shell occupations. The subscript outside the parentheses gives the total angular momentum for the state. The $(2p_{1/2}3s3p_{1/2})_{1/2}$ notation, for example, means a state with a $2p_{1/2}$ vacancy, one electron in the $3s$ orbital and

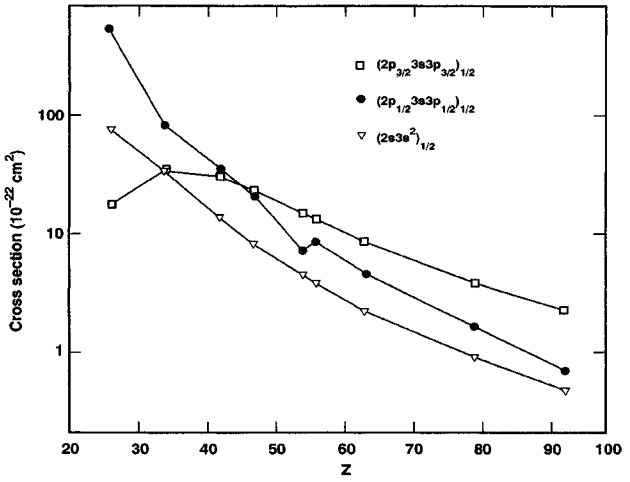

FIG. 1. Electron-impact-excitation cross sections for some intermediate states.

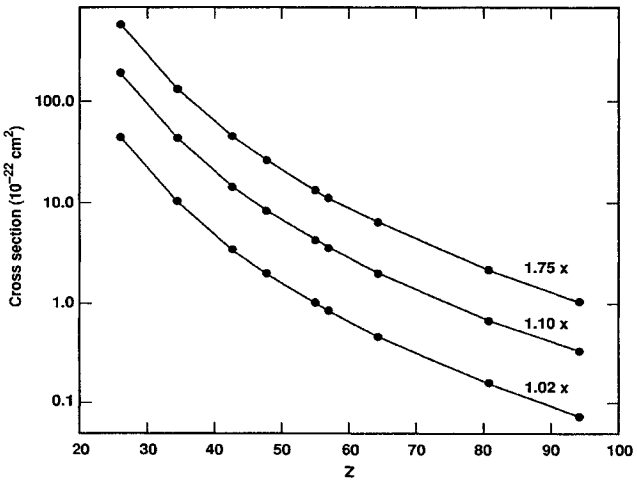

FIG. 2. Cross sections for direct ionization of $3s$ electron for Na-like ions at 1.02, 1.10, and 1.75 times the ionization threshold energy.

TABLE I. Ten largest excitation-autoionization cross sections for (a) Fe^{15+}, (b) Se^{23+}, (c) Mo^{31+}, (d) $Ag36^{+}$, (e) Xe^{43+}, (f) Ba^{45+}, (g) Eu^{52+}, (h) Au^{68+}, (i) U^{81+}. The numbers in square brackets denote powers of 10.

	Level	Configuration	B	Cross section (cm^2)
		(a) Fe^{15+}		
1	25	$(2p_{1/2}3s3p_{1/2})_{1/2}$	0.9885	4.825[−20]
2	66	$(2p_{1/2}3s3d_{5/2})_{3/2}$	0.5671	2.552[−20]
3	72	$(2p_{1/2}3s3d_{3/2})_{3/2}$	0.7979	2.050[−20]
4	23	$(2p_{1/2}3s3p_{3/2})_{1/2}$	0.9480	1.038[−20]
5	128	$(2s3s^2)_{1/2}$	0.9383	7.095[−21]
6	55	$(2p_{3/2}3s3d_{5/2})_{1/2}$	0.9584	6.851[−21]
7	54	$(2p_{3/2}3s3d_{5/2})_{3/2}$	0.4656	5.615[−21]
8	41	$(2p_{3/2}3s3d_{5/2})_{9/2}$	1.0000	4.588[−21]
9	11	$(2p_{3/2}3s3p_{3/2})_{7/2}$	1.0000	2.948[−21]
10	44	$(2p_{3/2}3s3d)_{7/2}$	0.7527	2.593[−21]
		(b) Se^{23+}		
1	35	$(2p_{1/2}3s3p_{1/2})_{1/2}$	0.9929	7.114[−21]
2	24	$(2p_{3/2}3s3p_{3/2})_{1/2}$	0.9765	6.887[−21]
3	74	$2p_{1/2}3s3d_{5/2})_{3/2}$	0.5864	5.864[−21]
4	49	$(2p_{3/2}3s3d_{5/2})_{3/2}$	0.6403	3.914[−21]
5	97	$(2p_{1/2}3s3d_{3/2})_{1/2}$	0.5762	3.775[−21]
6	116	$(2s3s^2)_{1/2}$	0.9866	3.054[−21]
7	18	$(2p_{3/2}3s3p_{3/2})_{1/2}$	0.9902	2.890[−21]
8	48	$(2p_{3/2}3s3d_{3/2})_{1/2}$	0.7925	1.562[−21]
9	39	$(2p_{1/2}3s3d_{5/2})_{9/2}$	1.0000	1.261[−21]
10	12	$(2p_{3/2}3s3p_{3/2})_{1/2}$	0.9887	7.959[−22]
		(c) Mo^{31+}		
1	39	$(2p_{1/2}3s3p_{1/2})_{1/2}$	0.9569	2.951[−21]
2	18	$(2p_{3/2}3s3p_{3/2})_{1/2}$	0.9856	2.531[−21]
3	48	$(2p_{3/2}3p^2_{3/2})_{3/2}$	0.7403	2.041[−21]
4	53	$(2p_{3/2}3p^2_{3/2})_{3/2}$	0.6053	1.249[−21]
5	112	$(2s3s^2)_{1/2}$	0.9870	1.198[−21]
6	52	$(2p_{1/2}3s3p_{3/2})_{1/2}$	0.9576	9.044[−22]
7	44	$(2p_{3/2}3s3d_{3/2})_{1/2}$	0.7648	7.923[−22]
8	111	$(2p_{1/2}3s3d_{3/2})_{3/2}$	0.3906	6.793[−22]
9	101	$(2p_{1/2}3s3d_{3/2})_{3/2}$	0.1861	6.419[−22]
10	51	$(2p_{3/2}3s3p_{5/2})_{1/2}$	0.2393	5.943[−22]
		(d) Ag^{36+}		
1	17	$(2p_{3/2}3s3p_{3/2})_{1/2}$	0.9796	1.918[−21]
2	48	$(2p_{1/2}3s3p_{1/2})_{1/2}$	0.9293	1.705[−21]
3	114	$(2s3s^2)_{1/2}$	0.9818	7.390[−21]
4	46	$(2p_{3/2}3p^2_{3/2})_{3/2}$	0.7561	4.084[−22]
5	49	$(2p_{3/2}3p^2_{3/2})_{3/2}$	0.8579	3.917[−22]
6	38	$(2p_{3/2}3p_{1/2}3p_{3/2})_{1/2}$	0.8334	3.178[−22]
7	43	$(2p_{3/2}3s3d_{5/2})_{3/2}$	0.0847	3.073[−22]
8	32	$(2p_{3/2}3s3d_{5/2})_{9/2}$	1.0000	2.876[−22]
9	47	$(2p_{3/2}3s3d_{5/2})_{1/2}$	0.1755	2.797[−22]
10	63	$(2p_{1/2}3s3p_{3/2})_{1/2}$	0.8652	2.770[−22]
		(e) Xe^{43+}		
1	18	$(2p_{3/2}3s3p_{3/2})_{1/2}$	0.9681	1.176[−20]
2	129	$(2s3s^2)_{1/2}$	0.9718	3.836[−21]
3	34	$(2p_{3/2}3p_{1/2}3p_{3/2})_{1/2}$	0.6861	1.810[−21]
4	32	$(2p_{3/2}3s3d_{5/2})_{9/2}$	1.0000	1.407[−21]
5	40	$(2p_{3/2}3s3d_{5/2})_{3/2}$	0.0407	1.076[−21]
6	184	$(2s3s3d_{5/2})_{7/2}$	0.9950	1.024[−22]
7	180	$(2s3s3d_{3/2})_{5/2}$	0.6079	9.076[−23]
8	11	$(2p_{3/2}3s3p_{3/2})_{7/2}$	0.9773	8.753[−23]
9	191	$(2s3s3d_{5/2})_{5/2}$	0.9130	7.134[−23]
10	113	$(2p_{1/2}3s3d_{3/2})_{3/2}$	0.8106	6.905[−23]

TABLE I. (*Continued*).

	Level	Configuration	B	Cross section (cm^2)
		(f) Ba^{45+}		
1	18	$(2p_{3/2}3s3p_{3/2})_{1/2}$	0.9641	1.057[−21]
2	64	$(2p_{1/2}3s3p_{1/2})_{1/2}$	0.9583	7.216[−22]
3	129	$(2s3s^2)_{1/2}$	0.9682	3.315[−22]
4	32	$(2p_{3/2}3s3d_{5/2})_{9/2}$	1.0000	1.275[−22]
5	181	$(2s3s3d_{5/2})_{7/2}$	0.9993	9.238[−23]
6	135	$(2p_{1/2}3s3d_{5/2})_{7/2}$	0.8840	6.929[−23]
7	180	$(2s3s3d_{3/2})_{5/2}$	0.4859	6.376[−23]
8	190	$(2s3s3d_{5/2})_{5/2}$	0.9275	6.186[−23]
9	39	$(2p_{3/2}3s3d_{5/2})_{1/2}$	0.0815	5.972[−23]
10	123	$(2p_{1/2}3p_{1/2}3p_{3/2})_{3/2}$	0.5478	5.538[−23]
		(g) Eu^{52+}		
1	18	$(2p_{3/2}3s3p_{3/2})_{1/2}$	0.9476	6.742[−22]
2	87	$(2p_{1/2}3s3p_{1/2})_{1/2}$	0.8564	3.571[−22]
3	127	$(2s3s^2)_{1/2}$	0.9499	1.855[−22]
4	32	$(2p_{3/2}3s3p_{3/2})_{1/2}$	0.7196	7.275[−23]
5	33	$(2p_{3/2}3s3d_{5/2})_{9/2}$	1.0000	7.247[−23]
6	181	$(2s3s3d_{5/2})_{7/2}$	0.9970	5.189[−23]
7	131	$(2p_{1/2}3p_{1/2}3p_{3/2})_{3/2}$	0.7351	4.905[−23]
8	140	$(2s3s3p_{1/2})_{3/2}$	0.6033	4.820[−23]
9	12	$(2p_{3/2}3s3p_{3/2})_{7/2}$	0.9492	4.453[−23]
10	117	$(2p_{1/2}3s3p_{3/2})_{1/2}$	0.8743	4.095[−23]
		(h) Au68+		
1	18	$(2p_{3/2}3s3p_{3/2})_{1/2}$	0.8962	2.578[−22]
2	120	$(2p_{1/2}3s3p_{1/2})_{1/2}$	0.8523	1.216[−22]
3	122	$(2s3s^2)_{1/2}$	0.9364	7.410[−23]
4	33	$(2p_{3/2}3s3d_{5/2})_{9/2}$	1.0000	2.200[−23]
5	166	$(2s3s3d_{5/2})_{7/2}$	1.0000	1.507[−23]
6	12	$(2p_{3/2}3s3p_{3/2})_{7/2}$	1.0000	1.449[−23]
7	134	$(2p_{1/2}3p_{1/2}3p_{3/2})_{3/2}$	0.1955	1.441[−23]
8	32	$(2p_{3/2}3p_{1/2}3p_{3/2})_{1/2}$	0.7375	1.420[−23]
9	29	$(2p_{3/2}3s3d_{3/2})_{7/2}$	0.7257	1.159[−23]
10	8	$(2p_{3/2}3s_{1/2}3p_{1/2})_{5/2}$	0.4801	1.015[−23]
		(i) U^{81+}		
1	18	$(2p_{3/2}3s3p_{3/2})_{1/2}$	0.8379	1.329[−22]
2	120	$(2p_{1/2}3s3p_{1/2})_{1/2}$	0.7802	5.387[−23]
3	122	$(2s3s^2)_{1/2}$	0.9064	3.656[−23]
4	165	$(2s3s3d_{5/2})_{7/2}$	0.9979	7.125[−24]
5	29	$(2p_{3/2}3s3d_{3/2})_{7/2}$	0.7625	5.074[−24]
6	32	$(2p_{3/2}3p_{1/2}3p_{3/2})_{1/2}$	0.7722	4.277[−24]
7	138	$(2p_{1/2}3p_{1/2}3p_{3/2})_{3/2}$	0.1258	3.174[−24]
8	135	$(2p_{1/2}3s3d_{3/2})_{3/2}$	0.0618	2.934[−24]
9	46	$(2p_{3/2}3s3d_{5/2})_{3/2}$	0.0085	2.580[−24]
10	170	$(2s3s3d_{5/2})_{5/2}$	0.8712	2.290[−24]

one electron in the $3p_{1/2}$ orbital, and a total angular momentum of $J=\frac{1}{2}$ for the state.

While different intermediate states appear in the tables for different ions, there are a few states which make prominent contributions in every ion. For example, the $(2p_{1/2}3s3p_{1/2})_{1/2}$ state makes a substantial contribution for each ion, as do the $(2s3s^2)_{1/2}$ state and the $(2p_{3/2}3s3d_{5/2})_{9/2}$ state. We were particularly interested in the $(2p_{3/2}3s3p_{3/2})_{1/2}$ state since we noted in Refs. [1] and [2] that this state makes the largest contribution to excitation autoionization in Au^{68+} and Xe^{43+}. This state has a large excitation cross section for both of these ions and in both ions this state has a large branching ratio (i.e., 0.896 and 0.996 in Au^{68+} and Xe^{43+}, respectively). In Au^{68+} this state accounts for nearly half of the total excitation-autoionization contribution. But it accounts

for only slightly more than one-third of the total in Xe^{43+}, even though the branching ratio is larger in Xe^{43+}. In Fe^{15+} this intermediate state contributes less than 1% of the total excitation-autoionization cross section. We made a detailed study of the way the contribution of some intermediate states changes along the isoelectronic sequence.

In Fig. 1 we show the electron-impact-excitation cross section as a function of atomic number for three intermediate states. In all cases the excitation cross sections are computed at an incident energy just above the excitation threshold. The excitation cross sections generally decrease rapidly with increasing atomic numbers. However, there are two notable exceptions. For the $(2p_{1/2}3s3p_{1/2})_{1/2}$ state the cross section for $Z=54$ is less than the cross section for $Z=56$; and for the $(2p_{3/2}3s3p_{3/2})_{1/2}$ state the cross section for $Z=26$ is about one-half the cross section for $Z=34$. In contrast to the cross section for the $(2p_{3/2}3s3p_{3/2})_{1/2}$ state, the cross section for the $(2p_{1/2}3s3p_{1/2})_{1/2}$ state in Fe^{15+} is nearly five times larger than this cross section for Se^{23+}.

In Fig. 2 we show the cross sections for direction ionization of the $3s$ electron for all of the ions. The ionization cross sections are shown for incident electron energies of 1.02, 1.10, and 1.75 times the ionization threshold energies. The direct ionization cross sections decrease smoothly and rapidly, dropping nearly three orders of magnitude between Fe^{15+} and U^{81+}.

Figure 3 shows the ratio of the excitation-autoionization cross sections to the direct ionization cross sections for the three intermediate states discussed above. In each case the excitation cross sections and the ionization cross sections are calculated at an energy just above the excitation threshold, and the excitation cross sections are multiplied by the branching ratio for the intermediate state. This ratio for the $(2p_{3/2}3s3p_{3/2})_{1/2}$ state starts out very low at $Z=26$ and rapidly increases with increasing atomic number. For Au^{68+} the excitation-ionization cross section for this single intermediate state is 2.7 times the direct ionization cross section, and in U^{81+}, the contribution of this state is more than 3.5 times the direct ionization contribution.

The ratio of B_iQ_i to Q_d for the $(2s3s^2)_{1/2}$ state is slightly higher than the $(2p_{3/2}3s3p_{3/2})_{1/2}$ cross section in the case of Fe^{15+}, but increases much more gradually with increasing Z. For $Z \geq 79$, the contribution of this state is about one-half the direct ionization contribution.

For the $(2p_{1/2}3s3p_{1/2})_{1/2}$ state the largest ratio of B_iQ_i to Q_d is for Fe^{15+}. For this ion the contribution of this intermediate state is equal to the direct ionization contribution and is much greater than the contribution of any other intermediate state. For the rest of the ions the contribution of this state varies between 70% and 100% of the direct ionization contribution, except for Xe^{43+}. At $Z=54$ the normalized cross section drops suddenly to 0.06, after reaching 0.95 at $Z=47$. It is back up to 0.96 at $Z=56$.

We noted earlier that a slight anomalous dip appears in the excitation cross section at $Z=54$ for the $(2p_{1/2}3s3p_{1/2})_{1/2}$ state. But this slight drop in the excitation cross section cannot account for the striking decrease in the excitation-autoionization cross section at $Z=54$. The reason for this decrease at $Z=54$ can be seen in Table II, where the branching ratios for the $(2s3s^2)_{1/2}$, $(2p_{3/2}3s3p_{3/2})_{1/2}$, and $(2p_{1/2}3s3p_{1/2})_{1/2}$ states are collected. The branching ratio for the $(2p_{1/2}3s3p_{1/2})_{1/2}$ state is 0.9293 for $Z=47$, and 0.9583 for $Z=56$, but for $Z=54$ it is 0.0846.

The dramatic drop in the branching ratio at $Z=54$ occurs because the $(2p_{1/2}3s3p_{1/2})_{1/2}$ eigenvector for Xe^{43+} has very large $(2p_{1/2}3s3d_{5/2})_{1/2}$ and $(2p_{1/2}3s3d_{3/2})_{1/2}$ coefficients. Very steep level crossings

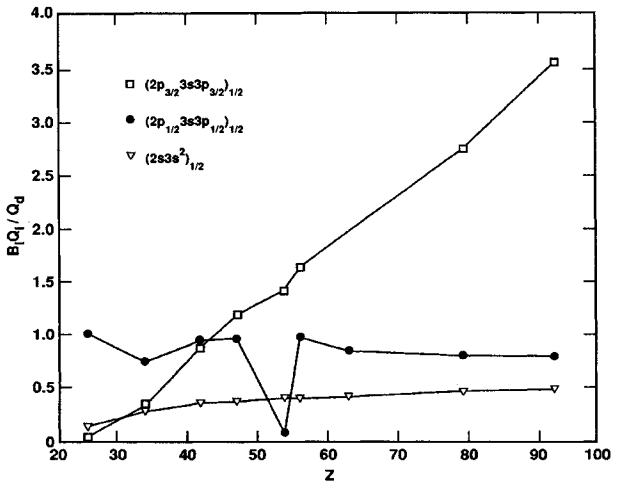

FIG. 3. Ratio of excitation-autoionization cross sections (B_iQ_i) to direct ionization cross sections (Q_d).

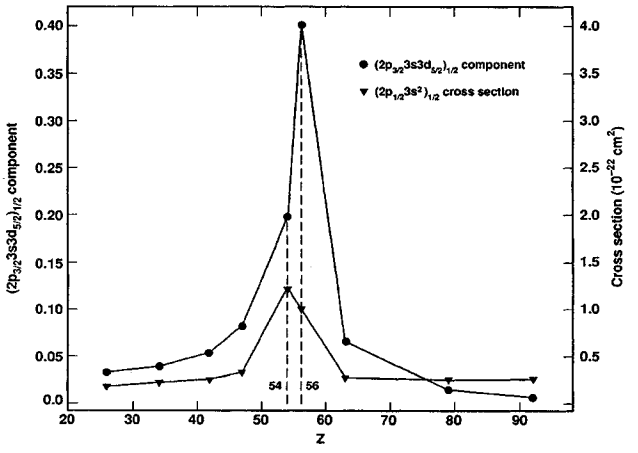

FIG. 4. $(2p_{3/2}3s3d_{5/2})_{1/2}$ component of $(2p_{1/2}3s^2)_{1/2}$ eigenvector and electron-impact excitation cross section for the $(2p_{1/2}3s^2)_{1/2}$ level for sodiumlike ions.

TABLE II. Branching ratios for the $(2s3s^2)_{1/2}$, $(2p_{3/2}3s3p_{3/2})_{1/2}$, and $(2p_{1/2}3s3p_{1/2})_{1/2}$ intermediate states.

	Branching ratios		
Z	$(2s3s^2)_{1/2}$	$(2p_{3/2}3s3p_{3/2})_{1/2}$	$(2p_{1/2}3s3p_{1/2})_{1/2}$
26	0.9383	0.9807	0.9985
34	0.9866	0.9902	0.9929
42	0.9870	0.9856	0.9569
47	0.9816	0.9796	0.9293
54	0.9718	0.9681	0.0846
56	0.9682	0.9641	0.9583
63	0.9499	0.9476	0.8564
79	0.9364	0.8962	0.8523
92	0.9164	0.8379	0.8379

occur for these states at $Z=54$, and hence strong configuration interaction among these states is manifested in Xe^{43+}. Both the $(2p_{1/2}3s3d_{5/2})_{1/2}$ state and the $(2p_{1/2}3s3d_{3/2})_{1/2}$ states have very large radiative decay rates, and the strong mixing with these two states at $Z=54$ results in the very small Auger branching ratio for the $(2p_{1/2}3s3p_{1/2})_{1/2}$ states in Xe^{43+}. In all of the other ions considered here the $(2p_{1/2}3s3p_{1/2})_{1/2}$ eigenvector has small coefficients for these other states.

Another interesting example of the effect of configuration interaction is noted for the $(2p_{1/2}3s^2)_{1/2}$ intermediate state. In Ref. [3] we pointed out that the excitation cross section for this state is relatively large in Xe^{43+}, but is relatively small in Fe^{15+} and Au^{68+}. The relatively large cross section for this state in Xe^{43+} is due to mixing of this state with the $(2p_{3/2}3s3d_{5/2})_{1/2}$ state. This $(2p_{3/2}3s3d_{5/2})_{1/2}$ level has one of the largest excitation cross sections among all of the intermediate states. In Fig. 4 the excitation cross section for the $(2p_{1/2}3s^2)_{1/2}$ state is plotted for all of the ions. The magnitude of the $(2p_{3/2}3s3d_{5/2})_{1/2}$ coefficient in the $(2p_{1/2}3s^2)_{1/2}$ eigenvector is also shown. This coefficient is very small in Fe^{15+}, i. e., (0.0335), and increases slowly with increasing Z. At $Z=54$ the coefficient rises steeply to 0.2005 and the $(2p_{1/2}3s^2)_{1/2}$ cross section also increases sharply. The magnitude of the $(2p_{3/2}3s3d_{5/2})_{1/2}$ coefficient is even larger (i.e., 0.4016) at $Z=56$. But at $Z=56$ the $(2p_{1/2}3s^2)_{1/2}$ excitation cross section is less than the cross section at $Z=54$. This decrease in the cross section occurs because the dominant $(2p_{1/2}3s^2)_{1/2}$ coefficient in the eigenvector and the $(2p_{3/2}3s3d_{5/2})_{1/2}$ coefficient have opposite signs in Ba^{45+}. In the case of Xe^{43+} and all of the lighter ions these two components have the same sign. These two coefficients also have opposite signs in Au^{68+}, but in this case the magnitude of the $(2p_{3/2}3s3d_{5/2})_{1/2}$ coefficient is sufficiently small that the effect is not very pronounced. Similar irregularities in the Auger rates of doubly excited $3l3l'$ states of sodium-like ions have been noted previously, and were explained as due to the effects of level crossings among various states [19].

In Fig. 5 the direct ionization cross sections, the total ionization cross sections without radiative decay, and the total ionization cross sections with radiative decay taken into account are shown for Se^{23+} and U^{81+}. The excitation-autoionization cross section for U^{81+} is dominated by a large increase near 8 keV, corresponding to the $(2p_{3/2}3s3p_{3/2})_{1/2}$ excitation. The contributions of the other intermediate states are small by comparison. In contrast to this, the Se^{23+} excitation-autoionization cross section exhibits a number of steplike increases. This illustrates a general trend. As Z increases along the Na-like sequence the excitation-autoionization contribution becomes increasingly concentrated in fewer and fewer transitions. In Fe^{15+} the ten largest excitation-

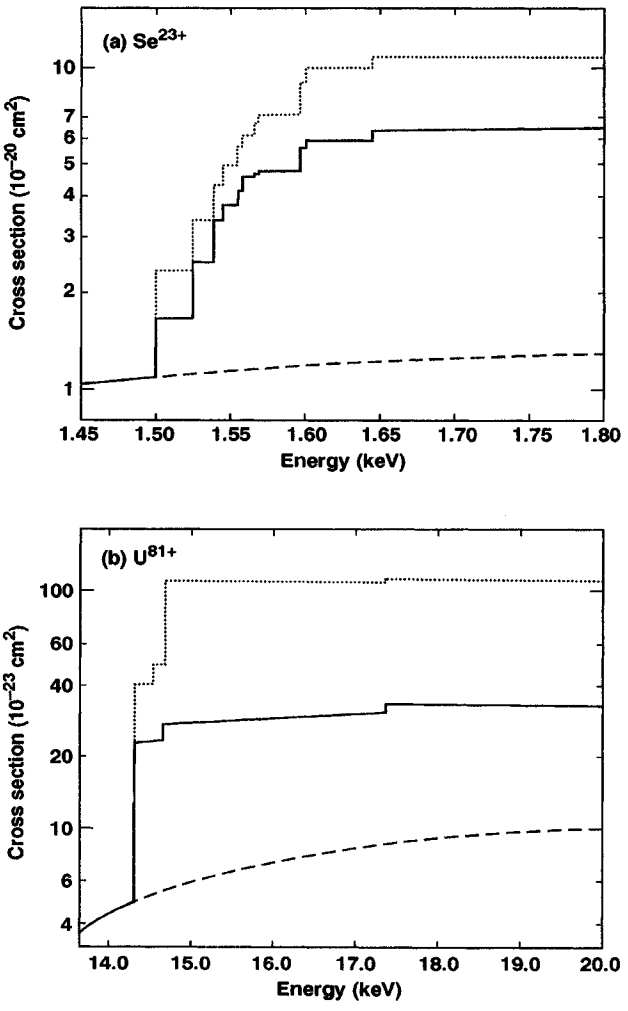

FIG. 5. Excitation-autoionization and direct ionization cross sections for (a) Se^{23+} and (b) U^{81+}: dashed curve direct ionization; dotted curve, total cross section with excitation-autoionization but without radiative decay; solid curve, total ionization cross section with allowance for radiative decay.

TABLE III. Effect of including Breit interaction in calculation of Auger rates. The numbers in square brackets denote powers of 10.

(a) Effect on intermediate states

Z	Level	Configuration	Branching ratio Without Breit interaction	Branching ratio With Breit interaction
34	12	$(2p_{3/2}3s3p_{3/2})_{7/2}$	5.846[−1]	9.987[−1]
34	31	$(2p_{1/2}3s3p_{3/2})_{3/2}$	1.981[−1]	2.439[−1]
54	26	$(2p_{3/2}3s3p_{3/2})_{3/2}$	8.338[−2]	1.033[−1]
54	31	$(2p_{1/2}3s3p_{3/2})_{3/2}$	5.144[−4]	2.785[−6]

(b) Effect on total excitation-autoionization contribution

Z	Total cross section (cm^2) Without Breit interaction	With Breit interaction
34	4.493[−20]	4.596[−20]
54	3.290[−21]	3.415[−21]

autoionization cross sections constitute about 70% of the total excitation-autoionization contribution; in Ba^{45+} the ten largest constitute almost 80% of the total; and in U^{81+} the ten largest constitute 97% of the total. The $(2p_{1/2}3s3p_{1/2})_{1/2}$ state, which makes the largest single contribution in Fe^{15+}, constitutes 25% of the total excitation-autoionization contribution in that ion. In contrast to this the largest single contribution in U^{81+}, which comes from the $(2p_{3/2}3s3p_{3/2})_{1/2}$ state, is more than 50% of the total excitation-autoionization contribution in this ion.

It can be seen in Figs. 5(a) and 5(b) that the effect of radiative decay is noticeably greater in U^{81+} than in Se^{23+}. This illustrates another trend in the isoelectronic sequence. The effect of radiative decay of the doubly excited states generally increases with increasing Z.

In our earlier work on excitation autoionization in Na-like ions (Refs. [1–3]), we did not include the Breit interaction in the calculation of the Auger rates. For the present work we examined the effect of this approximation. We found that for a few intermediate states, significant changes in the branching ratio resulted when the Breit interaction was included. Some of the branching ratios changed by several orders of magnitude. But the overall effect on the total excitation-autoionization cross sections was not significant. Table III illustrates these effects for Xe^{43+} and Se^{23+}.

In the earlier work we also neglected the effects of radiative decays among the $n=3$ states of the Na-like ions. We have included these radiative decays in the calculations reported in this paper. Since radiative rates increase rapidly as Z^4, one would expect that the effects of these $n=3$ to $n=3$ radiative decays to be most pronounced in the heaviest elements. In Table IV we show how the branching ratios and the excitation-autoionization cross section for the $(2p_{3/2}3s3d)_{9/2}$ intermediate state are affected by including these radiative decays. The effect for $Z=56$ is slightly larger than the

TABLE IV. Effect of including radiative decays among $n=3$ levels. The numbers in square brackets denote powers of 10.

(a) Effect on the $(2p_{3/2}3s3d_{5/2})_{9/2}$ level

Z	Branching ratio Without $n=3-3$ decays	Branching ratio With $n=3-3$ decays	Cross section (cm^2) Without $n=3-3$ decays	Cross section (cm^2) With $n=3-3$ decays
34	1.000 0	0.998 8	1.261[−21]	1.261[−21]
56	1.000 0	0.972 7	1.275[−22]	1.204[−22]
92	1.000 0	0.001 3	9.826[−24]	1.285[−25]

(b) Effect on total excitation-autoionization cross sections

Z	Total cross section (cm^2) Without $n=3-3$ decays	With $n=3-3$ decays
34	4.385[−20]	4.382[−20]
56	3.448[−21]	3.341[−21]
92	2.642[−22]	2.303[−22]

TABLE V. Total electron-impact ionization cross sections (direct ionization plus excitation-autoionization) for Na-like ions. The numbers in square brackets denote powers of 10.

Z	E_e (eV)	Total cross section (cm^2)
26	977.0	2.47[−19]
34	1 800.0	6.53[−20]
42	3 000.0	2.25[−20]
47	3 800.0	1.19[−20]
54	5 400.0	4.57[−21]
56	5 700.0	4.42[−21]
63	7 500.0	2.51[−21]
79	13 500.0	7.98[−22]
92	20 000.0	3.57[−22]

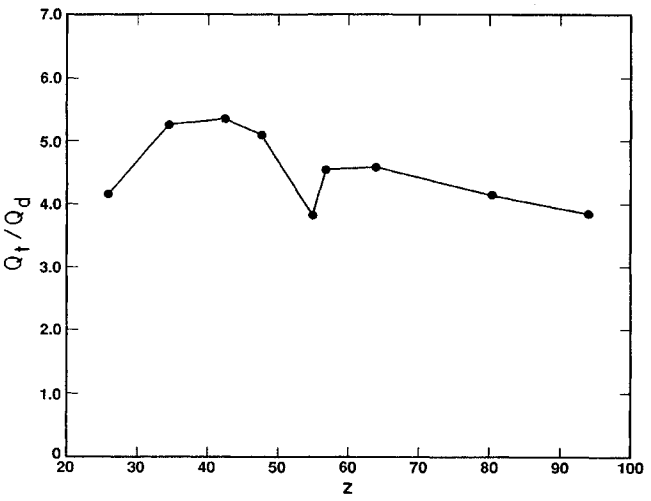

FIG. 6. Ratio of total ionization cross section to direct ionization cross section for sodiumlike ions.

nearly negligible effect for $Z=34$. But for $Z=92$, the branching ratio and the excitation-autoionization cross section decrease by more than an order of magnitude for this state. The overall effect on the total excitation-autoionization contribution is negligible for Se^{23+}, and only about 3% for Ba^{45+}. In U^{81+} where the effect is most pronounced, these radiative decays reduce the excitation-autoionization cross section by slightly more than 10%.

In Table V we give the total ionization cross sections for each of the ions studied. The variation in excitation-autoionization enhancement along the isoelectronic sequence can be seen in Fig. 6. We show the ratio of the total ionization cross section to the direct ionization cross section for the nine ions studied. This ratio is slightly more than 4 for Fe^{15+} and increases to about 5.4 for Mo^{31+}. It then decreases, reaching 3.8 for Xe^{43+}, which has the lowest enhancement. After increasing to 4.6 for Eu^{52+}, this ratio decreases for the remaining ions to slightly more than 3.8 for U^{81+}. The notable drop at $Z=54$ can be attributed to the configuration-interaction effects noted earlier for this ion. The decrease in the heavier ions, particularly U^{81+}, can be attributed to the effects of radiative decay.

CONCLUSIONS

We have used relativistic-distorted-wave methods to calculate cross sections for direct electron-impact ionization of the $3s$ electron in nine sodiumlike ions with $26 \le Z \le 92$. Relativistic-distorted-wave cross sections were calculated for electron-impact excitation of inner-shell $n=2$ electrons to $n=3$ levels of the ions, and detailed relativistic Auger rates and radiative rates were calculated in order to obtain branching ratios for the intermediate autoionizing states. We have investigated the variation of the excitation-autoionization contribution to the ionization cross section along the isoelectronic sequence. We found that for some of the ions, the cross sections for particular intermediate states are strongly affected by configuration interaction. This happens in ions where level crossings occur, and results in abrupt changes in the cross sections for the affected intermediate states. We found that including the Breit interaction in the calculation of the Auger rates can dramatically alter the branching ratios for some individual intermediate states, but does not significantly change the total excitation-autoionization cross sections. Similarly, including radiative decays among autoionizing states has little effect on the total cross sections, except for the very high Z ions where the effect is about 10%. There is some variation in the excitation-autoionization enhancement with increasing Z. The enhancement appears to be largest for $34 \le Z \le 47$ and appears to be lowest at $Z=54$. After this drop near $Z=54$, which appears to be due to configuration interaction, the increasing effects of radiative decay result in slowly decreasing enhancement for the heavier ions in the isoelectronic sequence.

ACKNOWLEDGMENT

This work was performed under the auspices of the U.S. Department of Energy by the Lawrence Livermore National Laboratory under Contract No. W-7405-ENG-48.

[1] K. J. Reed, M. H. Chen, and D. L. Moores, Phys. Rev. A **41**, 550 (1990).

[2] M. H. Chen, K. J. Reed, and D. L. Moores, Phys. Rev. Lett. **64**, 1350 (1990).

[3] K. J. Reed, M. H. Chen, and D. L. Moores, Phys. Rev. A **42**, 5315 (1990).

[4] R. D. Cowan and J. B. Mann, Astrophys. J. **232**, 940 (1979).

[5] K. T. LaGattuta and Y. Hahn, Phys. Rev. A **24**, 2273 (1981).
[6] D. C. Griffin, C. Bottcher, and M. S. Pindzola, Phys. Rev. A **25**, 154 (1982); **36**, 3642 (1987).
[7] R. J. W. Henry and A. Z. Msezane, Phys. Rev. A **26**, 2545 (1982).
[8] D. H. Crandall *et al.*, Phys. Rev. A **25**, 143 (1982).
[9] A. Müller and R. Frodl, Phys. Rev. Lett. **44**, 29 (1980).
[10] S. Andrianmonje *et al.*, Phys. Rev. Lett. **63**, 1930 (1989).
[11] E. D Donets, Phys. Scr. **T3**, 11 (1983).
[12] D. Schneider *et al.*, Phys. Rev. A **42**, 3889 (1990).
[13] D. L. Matthews *et al.*, Phys. Rev. Lett. **54**, 110 (1985).
[14] D. L. Moores and M. S. Pindzola, Phys. Rev. A **42**, 5384 (1990).
[15] H. L. Zhang and D. H. Sampson, Phys. Rev. A **42**, 5387 (1990).
[16] P. L. Hagelstein and R. K. Jung, At. Data Nucl. Data Tables **37**, 17 (1987).
[17] M. H. Chen, Phys. Rev. A **31**, 1449 (1985).
[18] I. P. Grant *et al.*, Comput. Phys. Commun. **21**, 207 (1980).
[19] M. H. Chen, Phys. Rev. A **40**, 2035 (1989).